LOCAL AND AVERAGE TRANSFER COEFFICIENTS
DUE TO AN IMPINGING ROW OF JETS

R. N. KOOPMAN and E. M. SPARROW

Department of Mechanical Engineering, University of Minnesota, Minneapolis, MN 55455, U.S.A.

Abstract—The local transfer coefficients which result from the impingement of a row of circular jets on a plane surface were determined by means of the naphthalene sublimation technique in conjunction with an innovative data acquisition system. Spanwise average and surface average transfer coefficients were also deduced from the local measurements. The parameters that were varied included the jet Reynolds number, the spacing between adjacent jet orifices, and the separation distance between the jet orifices and the impingement surface. The local transfer coefficient distributions enable the identification of surface locations where the impinging jets provide effective heating (or cooling). At locations that are mid-way between adjacent jets, relatively high local transfer coefficients may exist owing to the collision of the spreading flows from adjacent impinged jets. The stagnation point transfer coefficient exhibits a maximum as a function of the orifice-to-impingement separation distance. Both the spanwise average and surface average transfer coefficients take on their largest values on the impingement line and diminish with increasing downstream distance.

NOMENCLATURE

D,	jet orifice diameter;
$\mathscr{D}$,	diffusion coefficient;
K,	local mass-transfer coefficient, equation (1);
$\bar{K}$,	spanwise average mass-transfer coefficient, equation (3);
$\bar{\bar{K}}$,	surface average mass-transfer coefficient, equation (5);
$\dot{m}$,	local rate of mass transfer/area;
Re,	jet orifice Reynolds number, equation (6);
S,	center-to-center spacing between orifices;
Sc,	Schmidt number;
Sh,	local Sherwood number, equation (1);
$\overline{Sh}$,	spanwise average Sherwood number, equation (3);
$\overline{\overline{Sh}}$,	surface average Sherwood number, equation (5);
X,	streamwise coordinate;
Y,	spanwise coordinate;
Z,	separation distance between jet origin and impingement surface.

Greek symbols

μ,	viscosity;
ν,	kinematic viscosity;
ρ_{nw},	concentration of naphthalene vapor at plate surface;
$\rho_{n\infty}$,	concentration of naphthalene vapor in the free stream.

INTRODUCTION

IN RECENT years, the use of jet impingement as a high performance technique for heating or cooling a surface has become well established. The applications of the impingement technique are wide ranging and include,
for example, drying of paper, textiles and films deposited on substrates, annealing of metals, tempering of glass, cooling of electronic equipment, and freezing of tissue in cryosurgery. In many applications, where highly localized heating or cooling is required, a single jet is employed. On the other hand, when a larger expanse of surface is to be heated or cooled, it is necessary to use multiple jets. The two most frequently encountered jet configurations are slot jets and circular jets. The research to be reported in this paper is concerned with the latter.

There are basic differences in the fluid mechanics of single and multiple jets which, in general, preclude the use of single jet heat-transfer results for the design of multiple jet heating or cooling systems. In particular, the individual jets which comprise a multi-jet system may be influenced by two types of interactions which do not occur in the case of single jets. The first of these is the possible interference between adjacent jets prior to their impingement on the surface. The likelihood of such interference effects is enhanced when the jets are closely spaced and when the separation distance between the jet orifices and the impingement plate is relatively large. The second interaction is the collision of the surface flows (i.e. the wall jets) associated with adjacent impinged jets. These collisions are expected to be of increased importance when the jets are closely spaced, the jet orifice—impingement plate separation is small, and the jet velocity is large.

In the design of multiple jet impingement systems, the geometrical and flow parameters have to be selected to attain both a sufficiently high average heat-transfer coefficient and a degree of uniformity in the surface distribution that is adequate to avoid local hot (or cold) spots. The need for uniformity is especially important in applications involving drying, annealing, and tempering. It is also significant in the impingement cooling

of the internal walls of turbine blades. Basic information is, therefore, needed on the surface distribution of the local transfer coefficient as a function of the geometrical and flow parameters of the system.

The present research was undertaken in response to this need. Measurements were made of the local transfer coefficients associated with a row of circular jets impinging normal to a plane surface. These local results not only provide applicable numerical information, but also reveal the presence of a number of complex transfer mechanisms. In addition, by integration of the local transfer coefficients, results for the average transfer coefficients were obtained and are reported here. Measurements of the local transfer coefficients associated with a single impinging jet were also carried out for comparison purposes.

In view of the research objectives to obtain very localized and highly accurate transfer coefficients for well controlled boundary conditions, it was natural to consider the analogy between heat and mass transfer and, specifically, the naphthalene sublimation technique. For the present research, the impingement surfaces were naphthalene plates that had been painstakingly cast in a special mold. Local mass-transfer rates were determined from measurements of the surface contour of a plate both before and after exposure to jet impingement. Overall mass-transfer rates were obtained by direct weighing for comparison with the integrated local results.

The naphthalene technique has been used previously for simple jet impingement situations where the transfer coefficients depend only on one surface coordinate (e.g. [1, 2]), but never before for the complex two-dimensional distributions associated with multiple jet impingement. In view of the fact that these complex distributions require a large number (i.e. thousands) of local measurements for their accurate description, it was necessary to develop an innovative, semi-automated data acquisition system. One of the features of the system was that it significantly decreased the time needed to measure the surface contours of the naphthalene impingement plates compared with manual methods. This contributed to the accuracy of the results by reducing extraneous losses and eliminating human errors due to fatigue.

The local and average transfer coefficients will be presented in dimensionless form via the local and average Sherwood numbers, the values of which can be converted to Nusselt numbers by employing the analogy between heat and mass transfer. The boundary condition for the mass-transfer experiments corresponds to an isothermal impingement surface for the analogous heat-transfer problem. The parameters that were varied during the course of the experiments include the jet Reynolds number Re, the spacing S between the jet orifices, and the separation distance Z between the jet orifices and the impingement plate. The jet orifice diameter D was held fixed, and the geometrical parameters are reported via the ratios S/D and Z/D.

From a literature search, it appears that there is very little available information on local transfer coefficients for impingement of multiple circular jets and, in particular, nothing at all for a single row of circular jets. The heat-transfer measurements of Huang [3] for a multi-row array of impinging jets, although purported to be local, were actually averages. This is because the surface dimensions of the heat flux sensor used by Huang (1 × 1 in) were substantially larger than the diameter of the jet orifices (3/16 in) and the spacing between adjacent orifices (5/8 in center-to-center). Furthermore, the thermal boundary condition on the impingement surface was not controlled. Gardon and Cobonpue [4] used a small heat flux gage (0.9 mm dia) for studies of a square array of jets. Only sparse data are presented, the accuracy of which is in some doubt owing to a possible uncertainty in the calibration of the heat flux gage [5].

Information on average heat-transfer coefficients for impingement of a two-dimensional array of circular jets on a plane surface is reported in [3, 4, 6, 7]. For a single row of impinging jets, Metzger and Korstad [8] measured average heat-transfer coefficients in the absence of a cross flow as the initial phase of a study whose primary objective was to determine the influence of a superposed cross flow.

Certain aspects of the forthcoming presentation have been abbreviated to accommodate journal space limitations. Further details of the work are available in the thesis [9] on which this paper is based.

APPARATUS AND MEASUREMENT TECHNIQUE

The description of the experimental apparatus is facilitated by reference to Fig. 1, which is a schematic diagram showing a large test chamber within which the impingement surface is situated. The heart of the apparatus is the test section assembly consisting of the impingement plate and its supporting platform, the jet orifice plate, and a pair of side walls. The assembly is positioned in the upper part of the test chamber as indicated in the diagram.
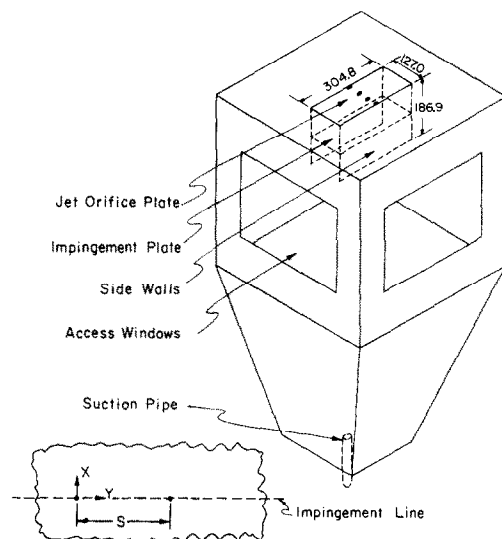

FIG. 1. Schematic diagram of the experimental apparatus.

Air from the laboratory room is drawn through the jet orifices. The jets are deflected by the impingement plate, thereby setting up a flow along the plate surface (i.e. a wall jet). The deflection is symmetric about the impingement line, so that there are mirror-image surface flows on the right- and left-hand halves of the impingement plate. Upon traversing the impingement plate, the flow empties into the test chamber proper, from which it is withdrawn by a downstream-positioned blower and ducted to a flow meter and finally to an exhaust at the roof of the building.

The experiments were intended to model a row of jets of sufficient spanwise extent so that end effects would not affect the measurements. To aid in achieving this objective, side walls were employed and semi-circular jet orifices (i.e. half orifices) were installed adjacent to each side wall. These measures proved to be fully successful, as will be demonstrated later.

The selection of the spacing between the jet orifices was, in part, made with end-effect considerations in mind. The arrangement shown in Fig. 1 was judged to provide the largest spacing consistent with negligible end effects. It corresponds to an S value of 42.34 mm (1.667 in) and an S/D of 6.67. The other spacing employed during the experiments is characterized by four full orifices flanked by the two half orifices, with $S = 25.40$ mm (1.000 in) and $S/D = 4$.

The jet orifices were designed and fabricated according to ASME orifice meter standards, with a 6.35 mm (0.250 in) orifice diameter and a downstream flare having a 60° included angle (see Fig. 4.4 of [9]). The thickness of the jet orifice plate is 1.524 mm (0.060 in).

The vertical position of the impingement-plate support platform is adjustable, thereby enabling the separation distance Z between the jet orifice plate and the impingement surface to be varied. In view of the fact that the jets are initiated at the upper surface of the orifice plate, Z is referred to that surface.

The naphthalene impingement plate rests on the support platform via four precisely machined stainless steel legs that are molded into the plate during the casting process. The naphthalene plate spans the full 127 mm width of the platform, but is somewhat shorter than the length of the platform. To continue the hydro-dynamic impingement surface, aluminum plates having height and width dimensions equal to those of the naphthalene plate were employed.

The casting of the naphthalene plates was a pains-taking procedure that is described in detail in [9]. In essence, the mold consists of a stainless steel base plate and four brass bars that serve as side walls. The stain-less steel plate had been precision ground, lapped, and hand polished to produce a smooth, flat, mirror-like surface (RMS roughness $\sim 6.35 \times 10^{-5}$ mm or 2.5×10^{-6} in). The back of the mold was open for pouring of molten naphthalene. Unmolding of the solidified naphthalene plate was accomplished by strategic hammer blows. Lubricants were never employed to assist unmolding, and the test surface, once produced, was never touched. Only fresh (not previously used) reagent grade naphthalene was used in the casting

process. All surfaces and edges of the cast naphthalene plate which do not participate in the mass-transfer process were covered with a pressure-sensitive tape to prevent extraneous sublimation and to avoid chipping or scraping.

Local mass-transfer rates were deduced from measurements of the surface contour of the naphthalene test surface both before and after an impingement data run. The measurements were performed with the naph-thalene plate situated on a movable coordinate table which enabled two directions of horizontal travel. The table was fitted with a guide and stops for positioning of the test plate. The contour measuring instrumen-tation was mounted on a strut which overhung the coordinate table.

The depth profiles were determined with the aid of instrumentation which converts the movement of a sensor tip (similar to the tip of a dial gage) into an electrical signal that can be read and recorded by a digital voltmeter. The instrumentation includes a sensing head which houses a linear variable differen-tial transformer and signal conditioning electronics. This sensing arrangement is capable of resolving surface elevations to within 2.54×10^{-4} mm (10^{-5} in). The linearity of the output voltage with elevation was investigated with the aid of Van Keuren gage blocks whose thickness had been determined to 10^{-5} in by the National Bureau of Standards. Linearity was found to prevail to $\frac{1}{2}\%$ in the measurement range of the present experiments. The circuitry for the contour sensing instrumentation is available in [9].

The overall mass transfer from an impingement plate was determined by before and after weighings made with a precision balance capable of discriminating to within 0.05 g for specimens having a mass up to 200 g. Air flow rates were measured with either of two calibrated rotameters, depending on the magnitude of the flow. Other instrumentation included a precision thermometer for air temperature (0.1C scale division), digital timer for measuring the various duration times needed to process the data (0.1 s scale division), and barometer and manometer for pressure measurements.

A number of precautions were taken in the design and conduct of the experiments in cognizance of the sensi-tivity of the vapor pressure of naphthalene to tem-perature (about 10%/°C at room temperature). The downstream placement of the blower precluded pre-heating of the air which might have occurred had the blower been upstream. The jet velocities were restricted to a maximum value of about 26 m/s (corresponding to $Re \sim 10000$) to limit the temperature rise due to stagnation and recovery (as well as to avoid erosion). To ensure thermal equilibrium with the temperature of the air in the laboratory room, the cast naphthalene plate (sealed under glass) was left in the room overnight; the room itself was temperature controlled. The outside exhaust system ensured that the room was free of naphthalene vapor.

The duration time of an impingement data run ranged from 10 to 30 min, depending on the Reynolds number and the geometrical parameters. The change of

surface elevation at the jet stagnation point due to sublimation during a data run was in the range 0.0254–0.0762 mm (0.001–0.003 in). The average change in elevation for the portion of the impingement plate for which data are to be reported was between 30 and 50% of that at the stagnation point.

ANALYSIS OF DATA

The data reduction procedures will be outlined briefly here, with full details available in [9].

The local differences between the surface contour measurements before and after a data run were employed, after correction, as the basis for the local mass-transfer rates and mass-transfer coefficients. Three corrections were carefully applied. The first and second were for natural convection sublimation that respectively occurred during the time when surface contour measurements were being made on the coordinate table and when the test section was being assembled. These corrections were determined from auxiliary *in situ* experiments. The third correction was for changes in surface elevation inherent in removing and subsequently repositioning of the naphthalene plate on the coordinate table. This positioning correction was made by employing the measured elevations of the exposed surfaces of the stainless steel legs as reference points. Since these surfaces do not participate in the mass-transfer process, any measured change in their elevations can be attributed to positioning.

The accuracy of the corrections is supported by the closure of the overall mass balance. For each data run, such a mass balance was evaluated by comparing the overall mass transfer obtained by direct weighing with that from a numerical integration of the local mass-transfer distribution. Typically, the closure was within 6%.

The corrected change in local surface elevation, when multiplied by the density of solid naphthalene and divided by the duration time of the data run, yields the local rate of mass transfer $\dot{m}(X, Y)$ per unit area. The X, Y coordinates are illustrated in the sketch at the lower left of Fig. 1. In this sketch, which is a view looking down on the impingement surface, the two blackened dots respectively represent the centerline positions of two adjacent impinging jets spaced apart by a distance S. The X and Y coordinates are, respectively, in the streamwise and spanwise directions.

The mass transfer is driven by the difference between the concentration of the naphthalene vapor at the wall and in the free stream, respectively denoted by ρ_{nw} and $\rho_{n\infty}$. The former is constant at all positions on the surface, since the wall temperature is constant. It was evaluated from the Sogin vapor pressure relation [10] in conjunction with the perfect gas law. The latter is zero for the present experiments.

Local mass-transfer coefficients K and Sherwood numbers Sh were evaluated from the definitions

$$K = \dot{m}/(\rho_{nw} - \rho_{n\infty}), \quad Sh = KD/\mathscr{D} \quad (1)$$

in which $\mathscr{D}$ is the naphthalene–air diffusion coefficient evaluated via the Schmidt number $Sc = v/\mathscr{D}$, where $Sc = 2.5$ [10] and v is the kinematic viscosity of air.

Two types of average mass-transfer coefficients were evaluated in order to help assess various aspects of the system performance. First, the spanwise average mass-transfer rate $\bar{\dot{m}}$ at each streamwise position X was found by trapezoidal rule integration

$$\bar{\dot{m}}(X) = [\int_0^{S/2} \dot{m} \, dY]/(S/2) \quad (2)$$

from which spanwise average coefficients were computed.

$$\bar{K} = \bar{\dot{m}}/(\rho_{nw} - \rho_{n\infty}), \quad \overline{Sh} = \bar{K}D/\mathscr{D}. \quad (3)$$

Next, the average transfer coefficient for the entire impingement surface between $X = 0$ and $X = X$ was obtained from

$$\bar{\bar{\dot{m}}}(X) = [\int_0^X \int_0^{S/2} \dot{m} \, dY \, dX]/(SX/2) \quad (4)$$

$$\bar{\bar{K}} = \bar{\bar{\dot{m}}}/(\rho_{nw} - \rho_{n\infty}), \quad \overline{\overline{Sh}} = \bar{\bar{K}}D/\mathscr{D}. \quad (5)$$

The Reynolds number used to parameterize the results was based on flow conditions at a jet orifice

$$Re = DG/\mu \quad (6)$$

in which G is the orifice mass velocity.

RESULTS AND DISCUSSION

The presentation of results will begin with a verification of spanwise and streamwise symmetry. Then, the results for the local transfer coefficients will be presented, followed by the average transfer coefficients and, finally, by a comparison of single and multiple jet results.

Symmetry

To illustrate the degree of symmetry attained in the present experiments as well as the absence of end effects, Fig. 2 has been prepared. The lower graph shows the variation of the sublimation depth as a function of spanwise position along the impingement line $X = 0$.
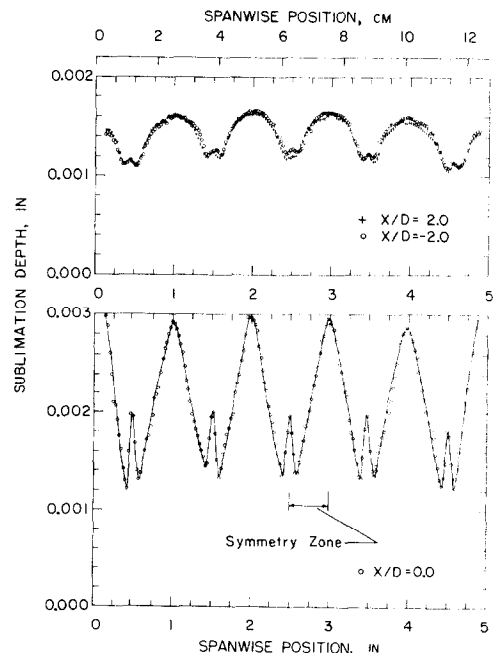

FIG. 2. Demonstration of spanwise and streamwise symmetry.

The spanwise symmetry evidenced by the data is excellent, and end effects are confined to the immediate neighborhood of the side walls. In view of this finding, subsequent data collection was restricted to the spanwise symmetry zone identified in the graph.

The upper graph contains two spanwise distributions, respectively for streamwise positions $X/D = 2$ and $X/D = -2$. The two distributions are nearly indistinguishable, thereby verifying that the impinging flow splits equally along the impingement line. For the subsequent runs, measurements were made only on the positive-X side of the impingement line.

Although the aforementioned findings are based on Fig. 2, which is for the $S/D = 4$ orifice spacing, identical findings were encountered for the $S/D = 6.67$ orifice spacing [9].

Local transfer results

The distributions of the local impingement-surface transfer coefficient contain a very large amount of numerical information, the extent of which is further enlarged by the presence of three independent parameters: Re, S/D, and Z/D. The most compact presentation that the authors were able to devise for these results is that of Figs. 3–10. The first four of these are for the $S/D = 4$ jet orifice spacing, whereas the last four are for the $S/D = 6.67$ spacing.

The successive Figs. 3–6 and 7–10 correspond to increasing orifice–impingement separation distances Z/D of 2, 4, 7 and 10. In each figure, there are several columns of graphs, with each column being for a
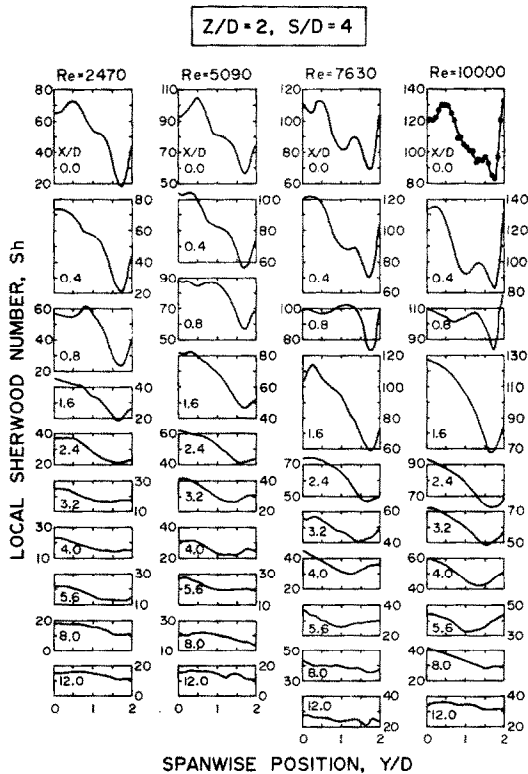

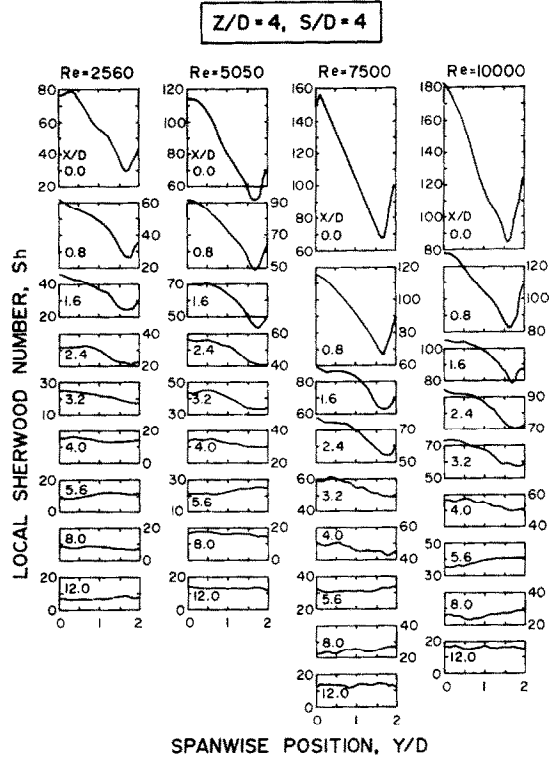FIG. 4. Local mass-transfer coefficient distributions, $Z/D = 4$ and $S/D = 4$.

FIG. 3. Local mass-transfer coefficient distributions, $Z/D = 2$ and $S/D = 4$.

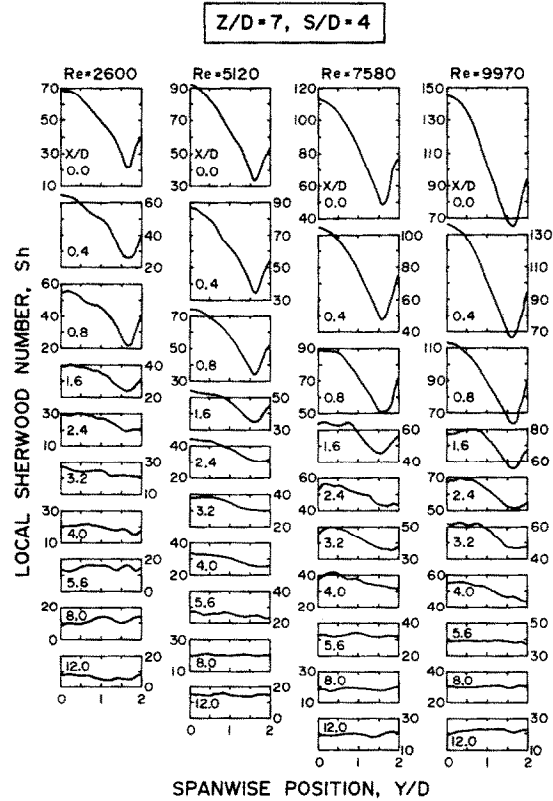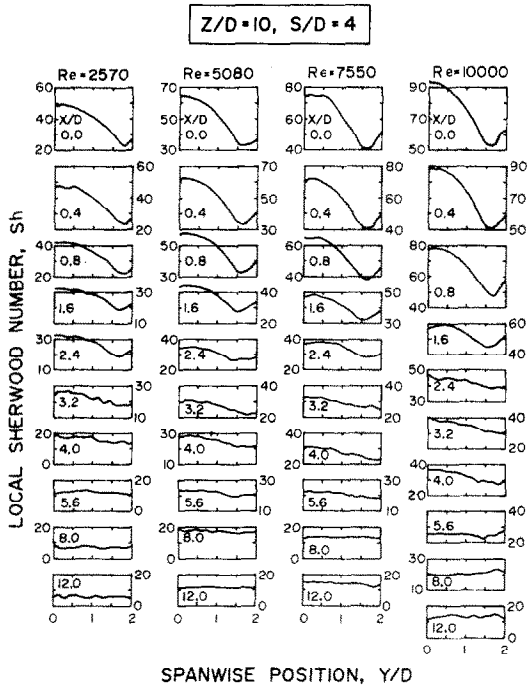FIG. 5. Local mass-transfer coefficient distributions, $Z/D = 7$ and $S/D = 4$.

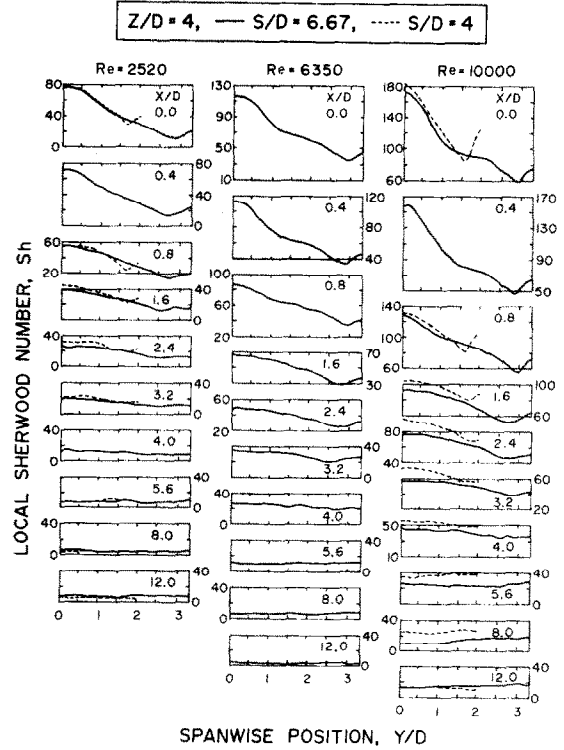FIG. 6. Local mass-transfer coefficient distributions,
$Z/D = 10$ and $S/D = 4$.

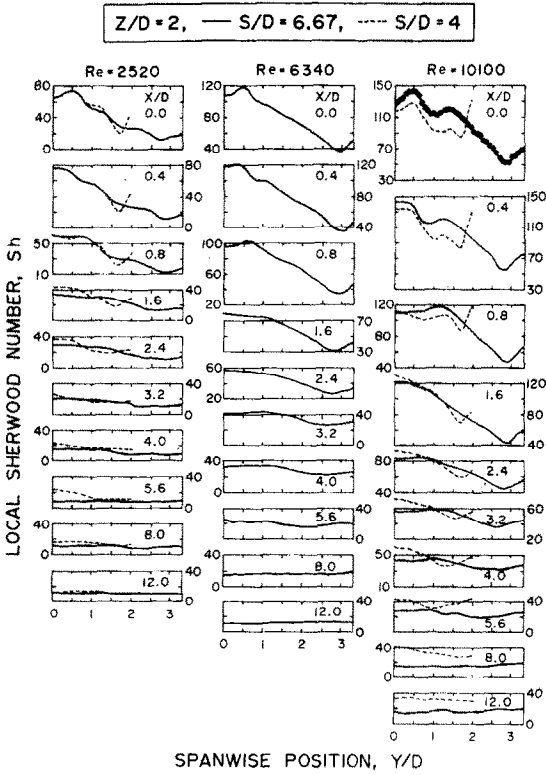FIG. 8. Local mass-transfer coefficient distributions,
$Z/D = 4$ and $S/D = 6.67$.

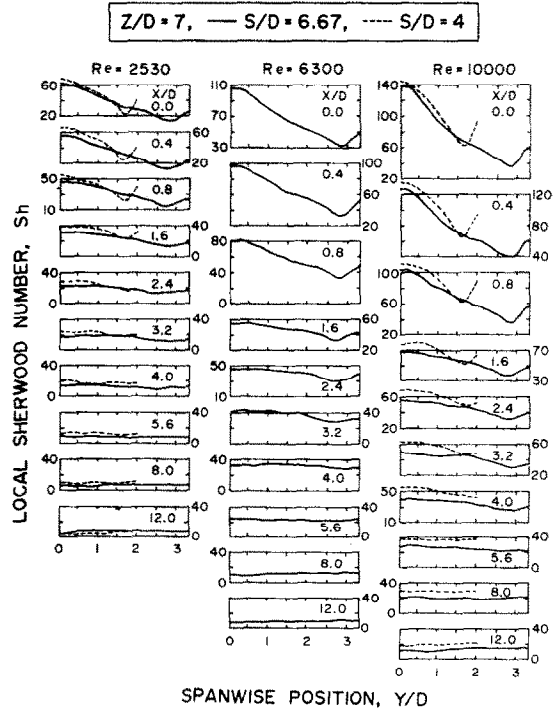FIG. 7. Local mass-transfer coefficient distributions,
$Z/D = 2$ and $S/D = 6.67$.

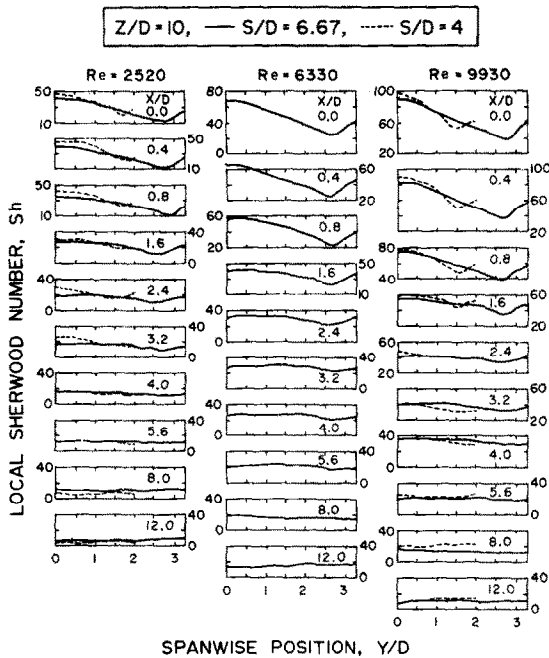FIG. 9. Local mass-transfer coefficient distributions,
$Z/D = 7$ and $S/D = 6.67$.

FIG. 10. Local mass-transfer coefficient distributions,
$Z/D = 10$ and $S/D = 6.67$.

specific Reynolds number. Each of the graphs shows the spanwise distribution of the local Sherwood number at a specific streamwise location X/D, and the successive graphs in a column correspond to a sequence of X/D locations starting at the impingement line $X/D = 0$ and increasing to $X/D = 12$. To simplify the presentation, data points are shown only in the graphs at the upper right of Figs. 3 and 7.

Examination of Figs. 3–10 reveals a highly complex set of distribution curves which require lengthy and thoughtful study to enable identification of trends. To begin, attention will be turned to the $S/D = 4$ spacing (Figs. 3–6). The results on and adjacent to the impingement line $X/D = 0$ contain a number of interesting features. One is the occurrence of a local maximum at $Y = S/2$, which is mid-way between adjacent jets. The presence of this maximum is due to the collision of the spreading flows from two impinged adjacent jets, and its prominence is accentuated at small Z/D separations and at larger jet Reynolds numbers. With increasing downstream distance, the collision-induced maxima tend to decay, the rapidity of the decay being dependent on both Re and Z/D.

A second interesting feature of the distribution curves at the impingement line is the presence of maxima at positions away from the stagnation point ($X = Y = 0$) in addition to the aforementioned maximum at $Y = S/2$. These off-stagnation maxima are in evidence at small Z/D separations (Figs. 3 and 4), particularly at $Z/D = 2$. Similar off-stagnation maxima were encountered in the single jet studies of Gardon and Akfirat [11]. The maximum at $Y/D = 0.5$, which may actually exceed the stagnation point transfer coefficient, can be attributed to a minimum in the boundary-layer thickness of the wall jet flow [12]. On the other hand, the maximum or, at lower Reynolds

numbers, the plateau that occurs in the region between $Y/D = 1$ and 1.5 is probably caused by transition to turbulence. These off-stagnation maxima and plateaus tend to manifest themselves at streamwise locations up to about $X/D = 1.6$ but are no longer in evidence at stations that are farther downstream.

With increasing downstream distance from the impingement line, the spreading of the impinged jets on the surface and the mixing of fluid from adjacent jets tends to homogenize the velocity field. This results in two-dimensional wall jet flow, which is essentially uniform across the span of the plate. As a consequence, the transfer coefficient distributions become independent of the spanwise coordinate and diminish in magnitude as the wall jet thickens with increasing X/D.

If comparisons are made from figure to figure among Figs. 3–6, it may be observed that the level of the transfer coefficients at a given X/D station does not vary monotonically with the Z/D separation distance. In particular, for stations between $X/D = 0$ and $X/D = 3$–4, the transfer coefficients at first increase as Z/D increases from 2 to 4 and then decrease for $Z/D = 7$ and 10. This finding will be explored more fully later.

Now, attention will be directed to Figs. 7–10. These figures serve two purposes. First, they portray the local Sherwood number results for the $S/D = 6.67$ spacing (solid lines). These results are given for three equally spaced Reynolds numbers covering the range from 2500 to 10000 (rather than the four Reynolds numbers of Figs. 3–6). Second, they include, for comparison purposes, dashed lines which represent the results for the $S/D = 4$ spacing for the two Reynolds numbers that are common to both spacings. These dashed lines are confined to the Y/D range from 0 to 2, which is the spanwise symmetry zone for the $S/D = 4$ spacing. The full range of the abscissa is from $Y/D = 0$ to 3.33, which is the symmetry zone for the $S/D = 6.67$ spacing.

A major difference in the results for the $S/D = 4$ and 6.67 spacings is in the nature of the Sherwood number maximum which occurs mid-way between adjacent impinged jets, respectively at $Y/D = 2$ and $Y/D = 3.33$. Except for the $Z/D = 10$ separation, the maximum is more prominent when the jets are more closely spaced. This is indicative of a more forceful collision of the spreading wall jet flows when the adjacent impinged jets are closer together. On the other hand, for $Z/D = 10$, the maximum appears to be somewhat more prominent when the jets are farther apart. This finding could be an indication of jet-to-jet interference before impingement, which would have a greater effect on the more closely spaced jets.

Another important difference is in the level of the transfer coefficients in the spanwise range between $Y/D = 2$ and 3.33, which is the incremental enlargement of the spanwise symmetry zone associated with an increase in jet orifice spacing from $S/D = 4$ to 6.67. For the $S/D = 4$ spacing, the part of the distribution curve that lies to the right of $Y/D = 2$ is the mirror image of that which lies to the left. These mirror image curves, which are not shown in the figures, fall well above the distribution curves for the $S/D = 6.67$

spacing, especially at streamwise positions where there are significant spanwise variations. Thus, a major impact of an increase in jet spacing is the decreased level of the transfer coefficients at spanwise positions which, because of the increased spacing, are situated farther from the impinging jets.

It is also interesting to compare the distribution curves for the two spacings in the spanwise range $Y/D = 0$ to 2. For $Re = 2500$, the two sets of distribution curves are not very different, except for the maximum at $Y/D = 2$ for the $S/D = 4$ spacing. On the other hand, the trends for $Re = 10000$ are more complex. At the closest Z/D separation and at positions on or near the impingement line, the Sherwood numbers for the more closely spaced jets are lower (Fig. 7, right-hand column). This is believed due to the particular behavior of the colliding wall jets at small jet orifice spacings and small orifice-to-impingement separations. Under these conditions and at high Reynolds numbers, the fluid that boils up due to collision may contact the jet orifice plate and, due to recirculation, interfere with the emerging free jet. Aside from the aforementioned situation, all of the other results for $Re = 10000$ are characterized by larger (or equal) Sherwood numbers for the more closely spaced jets. The distribution curves for the two jet orifice spacings are essentially identical for the $Z/D = 10$ separation.

As a final aspect of the local transfer results, consideration will now be given to the stagnation point $(X = Y = 0)$. In Fig. 11, the stagnation point Sherwood numbers are plotted as a function of the Z/D separation distance, with the Reynolds number as a parameter. In
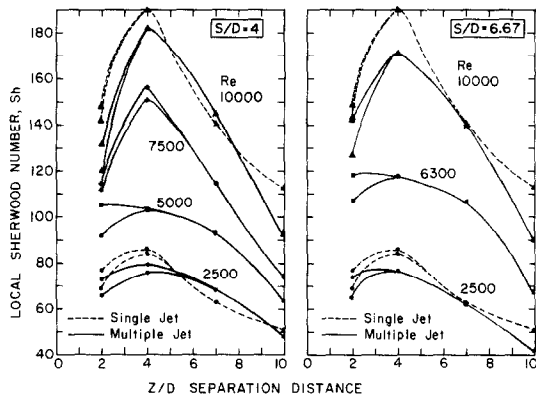

FIG. 11. Stagnation point mass-transfer coefficients.

addition to the results for the multiple jet configuration (solid lines), the figure also contains data for a single impinging jet (dashed lines). As additional information, the maximum Sherwood number in the stagnation region (which can occur at $Y/D = 0.5$ at the smaller Z/D) is also plotted if it differs from that at the stagnation point. This gives rise to the upper branch of the multi-branched curves.

The figure shows that there is a maximum in the stagnation point transfer coefficient as a function of the Z/D separation distance, and that the maximum becomes sharper at higher Reynolds numbers. The precise location of the maximum cannot be determined

from the available data, but it is probably in the range of Z/D between 4 and 6. Rathe han take arbitrary license in fairing the curves, the) .re drawn tightly through the data points, so that the apparent maximum is at $Z/D = 4$.

The existence of a maximum stagnation point transfer coefficient has already been noted for single jet impingement [4, 11, 13]. The maximum may be explained as follows. The initial increase of the transfer coefficient with Z/D is due to an increase of the turbulence level of the jet which results from entrainment and mixing. Once the potential core of the jet is engulfed by the entrainment process, the impingement velocity decreases and, subsequently, the turbulence also decreases. This brings about a decrease in the transfer coefficient.

Average transfer results

The spanwise average Sherwood number $\overline{Sh}$, which was evaluated from equations (2) and (3), provides a measure of the magnitude of the transfer coefficient along lines $X/D = $ constant, parallel to the impingement line. Results for $\overline{Sh}$ were obtained for both the $S/D = 4$ and 6.67 orifice spacings, but only the former are presented here to conserve space (see [9] for the latter).

The spanwise average results are shown in Fig. 12, where $\overline{Sh}$ is plotted as a function of X/D for parametric values of the Reynolds number and of the Z/D separation. The highest spanwise average coefficients are at the impingement line, except at closest separation where they occur along the line $X/D = 0.5$. With increasing distance from the impingement line, the coefficients decrease steadily. For instance, the coefficient on the line $X/D = 4$ is 35–50% of that at the impingement line, depending on the operating conditions.
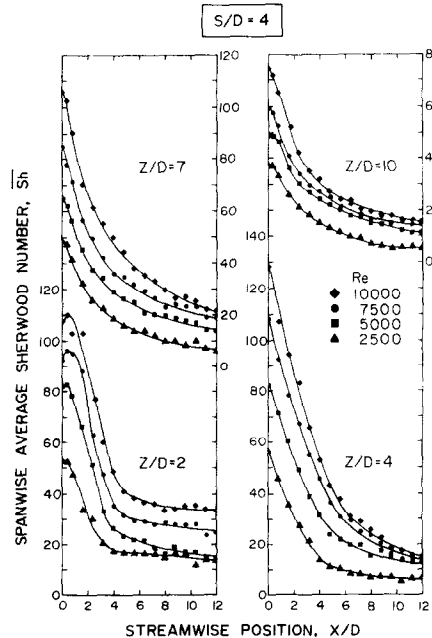

FIG. 12. Spanwise average mass-transfer coefficients, $S/D = 4$.

The results for the $Z/D = 2$ separation do not drop off to as low values as do those for the other separations. This is believed due to the close proximity of the jet orifice plate to the impingement surface, which may cause the flow at the larger X/D to behave like a duct flow rather than like a wall jet.

The surface average transfer coefficient for the portion of the impingement surface between $X = 0$ and $X = X$ was obtained from equations (4) and (5). The corresponding Sherwood numbers $\overline{Sh}$ are plotted in Figs. 13 and 14 as a function of the streamwise coordinate X/D which defines the downstream limit of the surface area over which the average is being taken. Figures 13 and 14 are, respectively, for $S/D = 4$ and 6.67.

The average Sherwood numbers are largest for those parts of the impingement surface that are situated in the neighborhood of the impingement line. As the averaging area encompasses more and more of the downstream portion of the impingement plate, the Sherwood number drops monotonically. Thus, for instance, for a section of impingement surface which extends from $X/D = 0$ to $X/D = 12$, the average Sherwood number is 30–50% of that at the impingement line, depending on the Reynolds number and the geometrical parameters.

A comparison of Figs. 13 and 14 reveals that the average coefficients for the $S/D = 4$ spacing are larger than those for the $S/D = 6.67$ spacing. Although the differences between the two sets of results vary with X/D and with the parameters, the global differences are about 25%.

The surface average coefficients are of particular relevance in impingement applications where the material to be heated or cooled is being moved under the row of jets. In particular, with the use of these results, the speed at which the material should be transported can be computed.

Single and multiple jet comparison

Measurements were made of the local impingement Sherwood numbers for a single circular jet at Reynolds numbers of 2500 and 10000 and for the same S/D and Z/D ranges as for the multiple jet experiments. Comparisons of the results for the single jet and the multiple jets are presented in [9] for all of these cases, but only a limited comparison, as presented in Fig. 15,
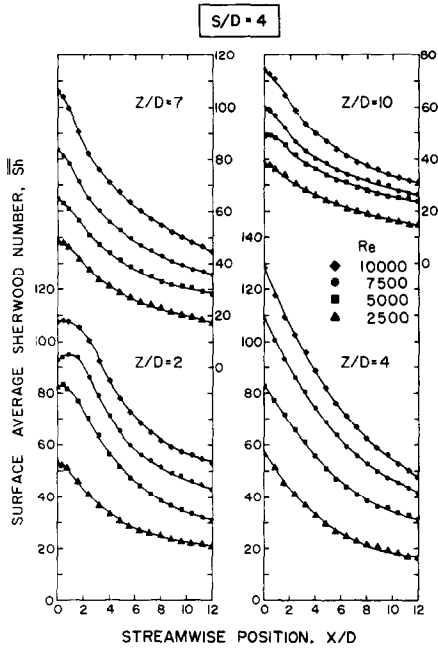

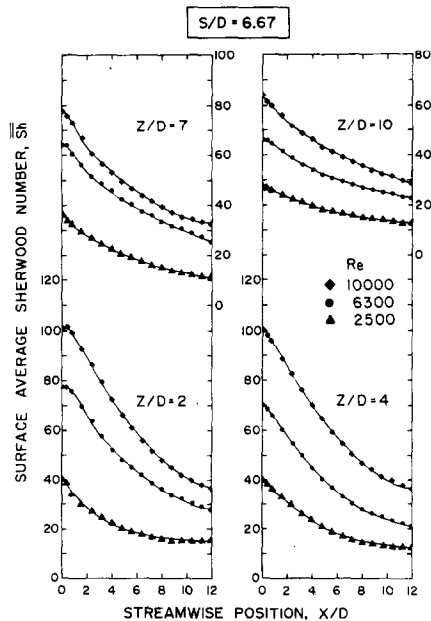FIG. 13. Surface average mass-transfer coefficients, $S/D = 4$.

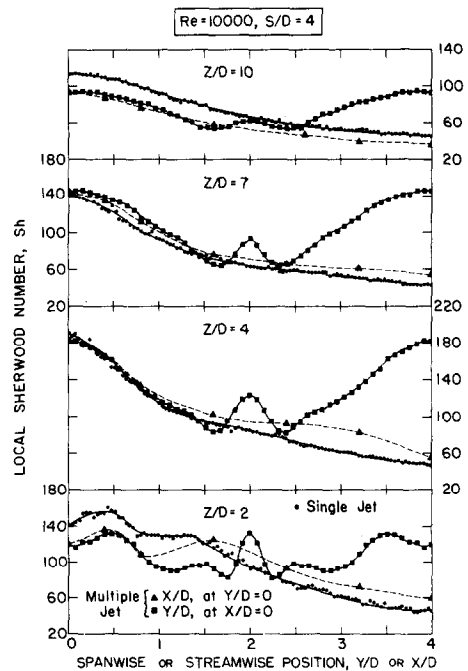FIG. 14. Surface average mass-transfer coefficients, $S/D = 6.67$.

FIG. 15. Comparisons of local mass-transfer coefficients for single jet and multiple jet impingement, $S/D = 4$ and $Re = 10000$.

can be made here owing to space limitations. The figure corresponds to a Reynolds number of 10000 and a jet orifice spacing $S/D = 4$. The local Sherwood number, which appears on the ordinate, is plotted against an abscissa which serves both as the spanwise coordinate Y/D and the streamwise coordinate X/D.

The single jet results (dots) depend only on the radial distance from the stagnation point and are, therefore, the same when plotted against Y/D or X/D. On the other hand, the local coefficients for the multiple jet system are different in the spanwise and streamwise directions and are designated by different symbols.

Within the multiple jet symmetry zone, $0 \leqslant Y/D \leqslant 2$, the spanwise distributions for the multiple jet case are below those for the single jet case except in the neighborhood of the collision zone and except at the $Z/D = 7$ separation. Beyond the symmetry zone, the multiple jet coefficients exceed those for the single jet. For the streamwise distributions, the comparison between the multiple and single jet results in the region between $X/D = 0$ and $X/D = 1.0-1.5$ is similar to that in the spanwise symmetry zone. For larger X/D, the multiple jet coefficients tend to be higher than those for the single jet due to the action of adjacent jets in inhibiting spanwise dispersion. The exception to this behaviour is the $Z/D = 10$ separation where the dissipation effect of jet-to-jet interference before impingement is believed responsible for the multiple jet results being low.

The present single jet results were compared in [9] with those of Gardon and Akfirat [11] for cases characterized by common values of the parameters. The agreement was found to be quite satisfactory.

CONCLUDING REMARKS

The naphthalene sublimation technique, used in conjunction with a semi-automated data acquisition system, has been shown to be a viable tool for determining the complex transfer coefficient distributions which result from multiple jet impingement. The complexity of the distributions requires that a large number of local measurements be made for their accurate description, and this is the reason why an effective data acquisition system is needed.

The local Sherwood number results enable the identification of surface locations where the impinging jets provide effective heating (or cooling) and where cold (or hot) spots may develop. Owing to the collision of the wall jets from adjacent impinged jets, the transfer coefficients at positions mid-way between the jets may take on relatively large values. The effect of such collisions is accentuated at high Reynolds numbers, small jet orifice spacings, and small orifice-to-impinge-

ment separations. At sufficiently large downstream distances, the spreading of the impinged jets and the mixing of fluid from adjacent jets produces a two-dimensional wall jet flow.

The stagnation point transfer coefficient exhibits a maximum as a function of the Z/D separation distance. The spanwise average transfer coefficients take on their highest value at the impingement line and diminish with downstream distance. At $X/D = 4$, the spanwise average coefficient is 35–50% of that on the impingement line. The surface average coefficients are largest when the averaging area is confined to the impingement line and diminish as the averaging area encompasses more and more of the downstream portion of the impingement plate. For a section of the impingement plate which extends from $X/D = 0$ to $X/D = 12$, the average coefficient is 30–50% of that at the impingement line.

REFERENCES

1. M. T. Scholtz and O. Trass, Mass transfer in a non-uniform impinging jet, *A.I.Ch.E. Jl* 16, 82–96 (1970).
2. M. Kumada and I. Mabuchi, Studies on the heat transfer of impinging jet, *Bull. J.S.M.E.* 13, 77–85 (1970).
3. G. C. Hwang, Investigations of heat transfer coefficients for air flow through round jets impinging normal to a heat transfer surface, *J. Heat Transfer* 85, 237–245 (1963).
4. R. Gardon and J. Cobonpue, Heat transfer between a flat plate and jets of air impinging on it, in *Proc. 1961 Int. Heat Transfer Conf.*, pp. 454–460. A.S.M.E., New York (1961).
5. R. Gardon and J. C. Akfirat, Heat transfer characteristics of impinging two-dimensional air jets, *J. Heat Transfer* 88, 101–108 (1966).
6. S. J. Freidman and A. C. Mueller, Heat transfer to flat surfaces, in *Proc. General Discussion on Heat Transfer*, pp. 138–142. Inst. Mech. Engrs., London (1951).
7. D. M. Kercher and W. Tabakoff, Heat transfer by a square array of round air jets impinging perpendicular to a flat surface including the effect of spent air, *J. Engng Power* 92, 73–82 (1970).
8. D. E. Metzger and R. J. Korstad, Effects of cross flow on impingement heat transfer, *J. Engng Power* 94, 35–41 (1972).
9. R. N. Koopman, Local and average transfer coefficients for multiple impinging jets, Ph.D. Thesis, University of Minnesota (1975).
10. H. H. Sogin, Sublimation from disks to air streams flowing normal to their surfaces, *Trans. Am. Soc. Mech. Engrs* 80, 61–71 (1958).
11. R. Gardon and J. C. Akfirat, The role of turbulence in determining the heat-transfer characteristics of impinging jets, *Int. J. Heat Mass Transfer* 8, 1261–1272 (1965).
12. S. P. Kezios, Heat transfer in the flow of a cylindrical air jet normal to an infinite plane, Ph.D. Thesis, Illinois Institute of Technology (1956).
13. J. W. Gauntner, J. N. B. Livingood, and P. Hrycak, Survey of literature on flow characteristics of a single turbulent jet impinging on a flat plate, NASA TN D-5652 (1970).

COEFFICIENTS DE TRANSFERT LOCAUX ET MOYENS D'UNE RANGEE DE JETS HEURTANT UNE PAROI

Résumé—Les coefficients de transfert locaux au contact d'une surface plane heurtée par une rangée de jets circulaires, one été déterminés à l'aide d'une technique de sublimation du naphtalène en relation avec un nouveau système d'acquisition de données. Les moyennes temporelles et moyennes surfaciques

des coefficients de transfert ont également été déduits des mesures locales. Les paramètres variables comprenaient le nombre de Reynolds des jets, la distance entre orifices de jets adjacents et la distance qui sépare l'orifice des jets à la surface recevant le jet. Les distributions des coefficients de transfert locaux permettent la détermination sur la surface des positions pour lesquelles le jet incident provoque un chauffage (ou un refroidissement) effectif. Aux positions situées à mi-chemin entre jets adjacents, des coefficients de transfert locaux relativement élevés peuvent exister du fait de l'intéraction entre écoulements de retour provenant de jets adjacents. Le coefficient de transfert thermique, en tant que fonction de la distance qui sépare l'orifice du jet à la surface frappée présente un maximum au point d'arrêt. Les coefficients de transfert moyens temporels et de surface deviennent maximum sur la ligne d'impact des jets et diminuent en aval de l'écoulement.

DER ÖRTLICHE UND MITTLERE WÄRMEÜBERGANGSKOEFFIZIENT BEIM AUFTREFFEN EINER REIHE VON STRAHLEN

Zusammenfassung—Der örtliche Wärmeübergangskoeffizient beim Auftreffen einer Reihe von Strahlen mit kreisförmigem Querschnitt auf eine ebene Oberfläche wurde mit Hilfe der Naphtalin-Sublimationstechnik zusammen mit einem neuartigen Datenerfassungssystem untersucht. Aus den örtlichen Meßwerten wurden die mittleren Wärmeübergangskoeffizienten ermittelt. Versuchsparameter waren die Reynoldszahl des Strahles, der Abstand zweier benachbarter Düsen sowie der Abstand zwischen Düsen und Auftreff-Fläche. Die Verteilung der örtlichen Wärmeübergangskoeffizienten ermöglicht die Bestimmung derjenigen Oberflächenbereiche, wo die auftreffenden Strahlen eine effektive Heizung (oder Kühlung) bewirken. An den zwischen 2 Düsen liegenden Stellen können infolge des Zusammentreffens zweier Strahlen relativ hohe örtliche Wärmeübergangskoeffizienten auftreten. Der Wärmeübergangskoeffizient im Staupunkt zeigt ein Maximum, das vom Abstand zwischen Düse und Auftreff-Fläche abhängig ist. Die mittleren Wärmeübergangskoeffizienten erreichen ihre höchsten Werte dort, wo die Strahlen zusammentreffen und nehmen mit zunehmender Entfernung von der Düse ab.

ЛОКАЛЬНЫЕ И СРЕДНИЕ КОЭФФИЦИЕНТЫ ПЕРЕНОСА ПРИ НАЛИЧИИ СИСТЕМЫ ПАДАЮЩИХ НА ПОВЕРХНОСТЬ СТРУЙ

Аннотация — Методом сублимации нафталина с помощью новой системы обработки данных определялись локальные коэффициенты переноса при набегании системы круглых струй на плоскую поверхность. Средние по ширине струи и по поверхности значения коэффициентов переноса определялись также по локальным замерам. Меняющиеся параметры включали число Рейнольдса для струи, расстояние между двумя соседними форсунками и расстояние между форсунками и поверхностью ударения струй. Распределения локальных значений коэффициента переноса позволяют определить области эффективного нагрева (или охлаждения на поверхности) с помощью падающих струй. На середине расстояния между соседними струями могут иметь место относительно высокие локальные значения коэффициентов переноса из-за соударения соседних расходящихся падающих струй. Коэффициент переноса в критической точке имеет максимальное значение в зависимости от расстояния между форсункой и твердой преградой. Как средние по ширине струи, так и по поверхности коэффициенты переноса имеют максимальные значения на линии падения и уменьшаются с увеличением расстояния вниз по потоку.